

# **AlGaN Material Structures for a Two Color UV Imager**

**Final Report**  
**Project #: NNG05GK57G**

Muhammad Jamil and Ian Ferguson  
School of Electrical Engineering  
Georgia Institute of Technology  
Atlanta, Georgia 30332-250 U.S.A  
Phone: 404-385-2885  
Email: [ianf@ece.gatech.edu](mailto:ianf@ece.gatech.edu)

## Summary:

GaN/AlGaIn dual-band detectors responding in UV and IR regions based on interband and intraband transitions have been developed. These dual-band detectors simultaneously detect UV radiation in the 250–360 nm and IR radiation in the 5–14  $\mu\text{m}$  regions with near zero spectral cross talk. MOCVD growth and process conditions were optimized for GaN and AlGaIn thin films as well as for device structures to improve the efficiency of devices. Also, by etching out the top-contact layer, it was shown that the UV response of the detector can be enhanced. Having separate UV- and IR-active regions with three contacts (one common contact for both regions) allows the separation of the UV and IR generated photocurrent components, identifying the relative strength of each component. This is an important development in UV–IR dual-band applications such as fire–flame detection, solar astronomy, and military sensing, eliminating the difficulties of employing several individual detectors with separate electronics–cooling mechanisms.

### 1.1 GaN/AlGaIn growth and process optimization:

The AlGaIn epitaxial layers were grown in a low pressure, vertical injection MOCVD reactor on *c-plane* sapphire. Trimethylgallium (TMGa), trimethylaluminum (TMAI), and ammonia were used as Ga, Al, and N precursors, respectively. The substrate was initially treated in  $\text{H}_2$  ambient at 1100  $^\circ\text{C}$  for 10 min. Then, 25 nm thick GaN buffer layers at 500  $^\circ\text{C}$  followed by 2  $\mu\text{m}$  thick undoped GaN layer were grown at 1050  $^\circ\text{C}$ . The metalorganic sources and ammonia were injected into the reactor by separate gas lines, and a relatively low pressure (50 Torr) was used to avoid pre-reactions between the alkyls and the hydrides.  $\text{H}_2$  and  $\text{N}_2$  were used as carrier gases during AlGaIn growth. The Al content in the AlGaIn layers was calibrated by changing the Al/Ga molar flow ratio during material growth. It was found that the growth temperature and reactor pressure can influence the Al content in AlGaIn alloys under the same Ga/Al molar flow ratio. After material growth, the Al content in AlGaIn alloys was confirmed by X-ray diffraction. Optimization of GaN-AlGaIn surface morphology (AFM) for intrinsic and doped layers was performed for each layer. Similarly, structural (XRD), optical (PL) and electrical (Hall) analysis of the GaN-AlGaIn layers and heterostructures was conducted to estimate the structural and optical defect concentrations and correlated those with the growth parameters.

To understand and overcome the present limitations in the dual-band detector performance, the origin and roles of dislocations in the GaN-AlGaIn device structures were studied with transmission electron microscope (TEM) and x-ray diffraction (XRD). It was found that the majority of the dislocations are originating from the initial nucleation layer. Even though the dislocation density is largely reduced within the first micron of the GaN template layer, the remaining dislocation density still has to be reduced in order to improve the signal to noise ratio of UV-IR detectors. The high dislocation density in the device structure is certainly a main source for the high dark leakage current in the detector structures. In a single heterojunction device structure, the mean-free path length might be still sufficient for minority carrier separation and collection. However, an increase in the number of scattering centers in a multiple layer detector structure will lead to a significant reduction of quantum efficiency and operation temperatures. A significant detector device improvement was accomplished by optimization the

processing conditions of the GaN template on sapphire as well as the subsequent layers of the device structure.

## 1.2 Characterization of optimized GaN/AlGaN films:

The growth conditions of the undoped GaN layers were optimized to reduce the background carrier concentration in the films. The optimized GaN films have a carrier concentration of  $-7.7 \times 10^{15} \text{cm}^{-3}$ , which is a very good background concentration for undoped GaN films. The lowest possible background carrier concentration in undoped GaN films allows for predictable behavior when they are doped for n-type conductivity. The n-type doping of GaN films was calibrated to achieve electron concentration up to  $8.3 \times 10^{18} \text{cm}^{-3}$ . The photoluminescence (PL) of undoped and n-type films was performed to assess the optical quality of the films. A high band edge versus yellow luminescence ratio, Figure 1 (a, b) in the undoped films shows very good optical quality of the films. Following undoped and n-type GaN, AlGaN films were also optimized for Al content as well as for the crystal quality of the films.

The Al content increases almost linearly from 2% to 6% for the TMAI flow rate of 15-100 sccm while the AlGaN growth rate was found to decrease with increasing Al flow rate. Also, the Al content in AlGaN layer is increased when the growth temperature is increased from 1050°C to 1070°C; while other growth parameters remained identical. Figure 2(a) shows  $2\theta$ - $\omega$  scan of optimized GaN template with a FWHM of 284 arcsec, indicating good crystal quality of the films. Next, varying composition AlGaN films were grown and optimized at different chamber pressures. The Al content was also found to increase with decreasing reactor pressure, possibly due to the suppression of pre-reactions between TMAI and  $\text{NH}_3$ , as shown in Figure 2(b). After calibration process, high crystal quality AlGaN layers with Al composition up to 26% have been achieved.

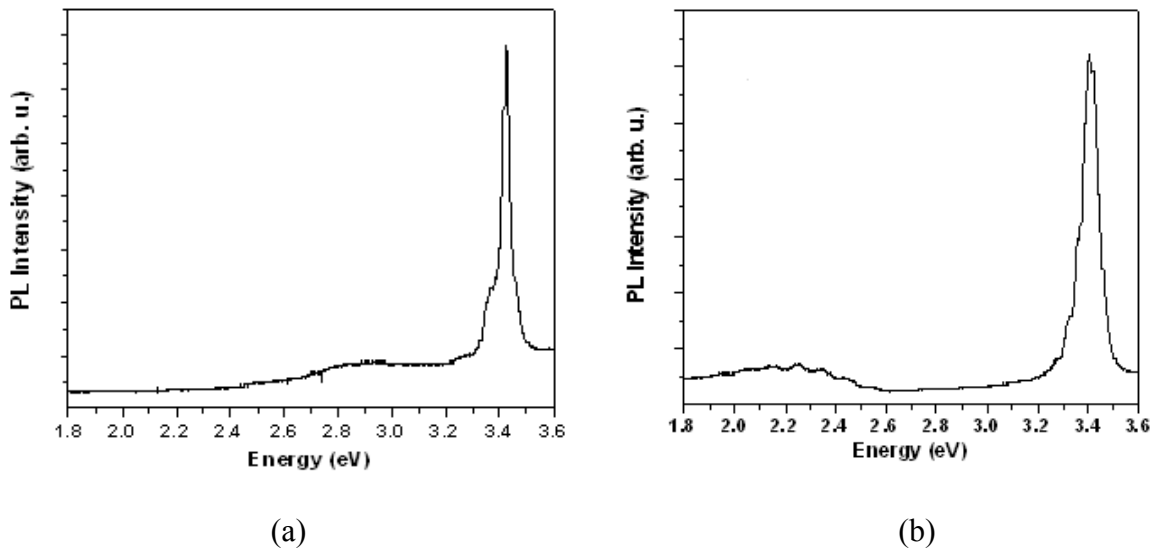
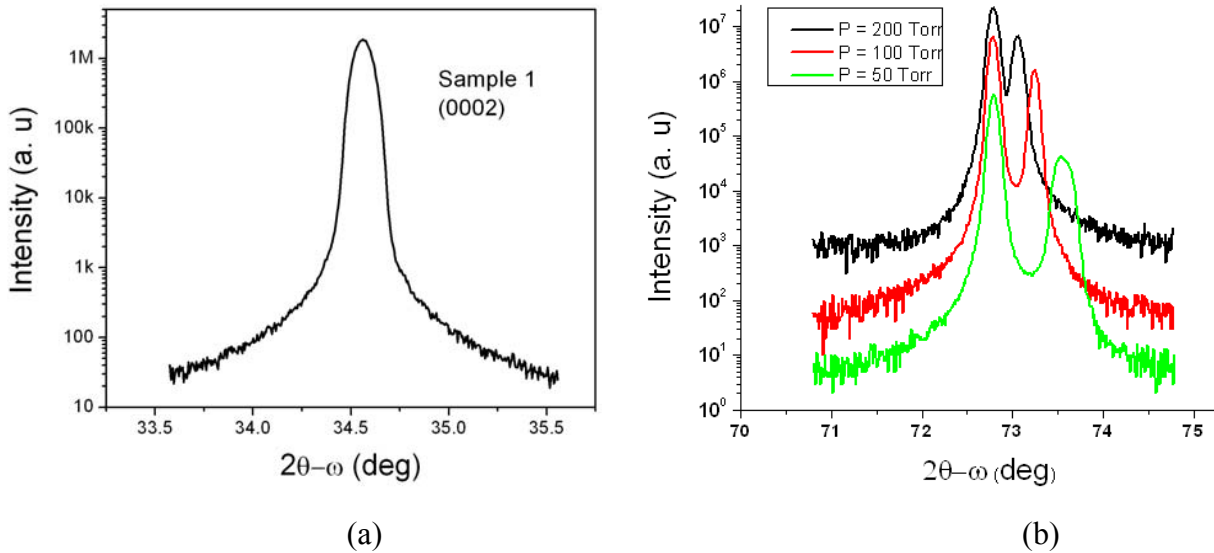


Figure 1: Room temperature photoluminescence spectra of (a) undoped GaN and (b) n-type GaN.



**Figure 2:** X-ray diffraction 2theta-omega scan of (a) GaN template (b) varying composition AlGaIn films grown at different pressures.

### 1.3 Device fabrication and results:

Following the thin film growth and process optimization, GaN/AlGaIn device structures were grown and fabricated. The structures were processed to form square mesa elements with different active areas by dry etching techniques. The ohmic contacts were formed by deposition of Ti/Al/Ti/Au (metalization) on the top- and bottom-contact layers. After the metalization, the device structures were annealed in  $N_2$  ambient at  $700^\circ C$  for two minutes. The annealed samples were mounted on chip carriers and wire bonds were made from each mesa of the sample to the chip carrier. Current-voltage (IV) measurements were performed, by using a Keithley 2400 source meter, on all the mesas of the sample in order to check for uniformity of the structure. The spectral response of the detector in the UV region was obtained using an Oriel Deuterium UV source, UV/VIS monochromator, and neutral density filters, and spectra were calibrated using a background spectrum obtained by a Hamamatsu photomultiplier tube with a known sensitivity. Spectral measurement in the IR region for normal incidence radiation were carried out by using a Perkin Elmer System 2000 Fourier transform infrared (FTIR) spectrometer. The spectra were calibrated relative to a background spectrum obtained by a Si composite bolometer with the same set of optical components.

The dual-band detection mainly involves two detection mechanisms. The UV detection is based on interband transitions of carriers in the  $Al_{0.026}Ga_{0.974}N$  barrier, while the IR detection is due to intraband transitions of free carriers in the emitter. The typical detector design and energy band diagram indicating the transitions due to both mechanisms is depicted in Figure 3. The intraband detection IR mechanism involves free carrier absorption in the emitter, followed by the internal photoemission of photoexcited carriers across the junction barrier, and then the collection of carriers by the applied electric field at the contacts.

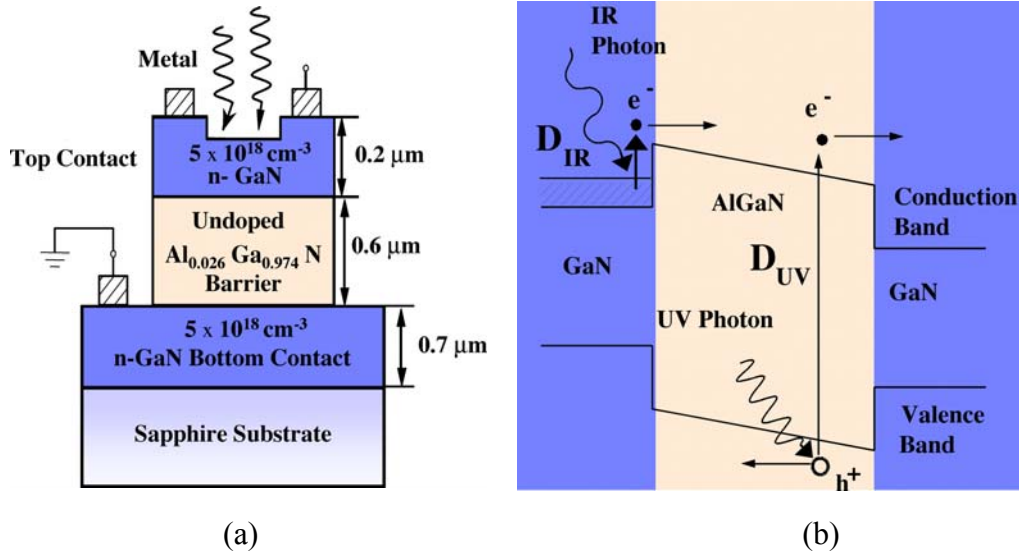


**Figure 3:** (a) Schematic diagram of GaN/AlGaIn structure. The emitter top contact and the bottom contact are doped to  $5 \times 10^{18} \text{ cm}^{-3}$  with Si as the  $n$ -type dopant, while the  $\text{Al}_{0.026}\text{Ga}_{0.974}\text{N}$  barrier is not intentionally doped. (b) The band diagram showing the conduction/valence band profile of the structure and the transitions leading to UV and IR responses.

The results of GaN/AlGaIn dual-band detectors responding in UV and IR regions based on interband and intraband transitions in the structure have been published [1, 2]. The UV threshold is observed at 360 nm, and the IR response is in the range 3–13 μm as shown in figure 4. The broad peak in the 11–13.6 μm region superimposed on the free carrier response is assigned to transitions related to carbon or nitrogen states [3, 4]. The reported donor ionization energy of carbon falls in the 110–140 meV range, while the binding energy of N vacancy is about 100 meV. Assuming that the two peaks observed at 11.9 μm (104.2 meV) and 13.3 μm (93.2 meV) are due to transitions of excited carbon states, the ionization energies were calculated to be 139 and 124 meV, respectively. These ionization energy values in the 140–110 meV range support the assumption that the corresponding transitions are carbon donor related impurity transitions. As peak at 54 μm (5.5 THz) is also observed in the response spectrum. The corresponding energy for transitions leading to this peak is 23 meV. This response peak can be identified as  $1s-2p_{\pm}$  transition of Si donors in GaN. These results imply that GaN provides the advantage of developing a 5.5 THz (54 μm) detector, based on the  $1s-2p_{\pm}$  transition of Si in GaN. On the other hand, the Si impurity-related transition can lead to an increased dark current for a detector designed to operate in a shorter wavelength region.

In the dual-band detector developed above, both photocurrent components were collected from the same two terminals. This limits the usefulness of the detector due to the inability of determining which wavelength was detected (UV, IR, or both). Next, dual-band detector was developed which has separate UV- and IR-active regions with three contacts (one common contact for both regions) for separate and simultaneous measurements of the UV- and IR photocurrent components [5]. The structure consisted of an  $n^+$ -GaN top-contact (TC) layer, an undoped  $\text{Ga}_{0.974}\text{Al}_{0.026}\text{N}$  layer acting as the UV-active region, an  $n^+$ -GaN middle-contact (MC) layer, the IR-active region, and a bottom-contact (BC) layer. The IR-active region consists of two periods of an  $n^+$ -GaN emitter layer and an undoped  $\text{Ga}_{0.974}\text{Al}_{0.026}\text{N}$  barrier layer. Depending on the bias either the MC or the BC also acts as an emitter.

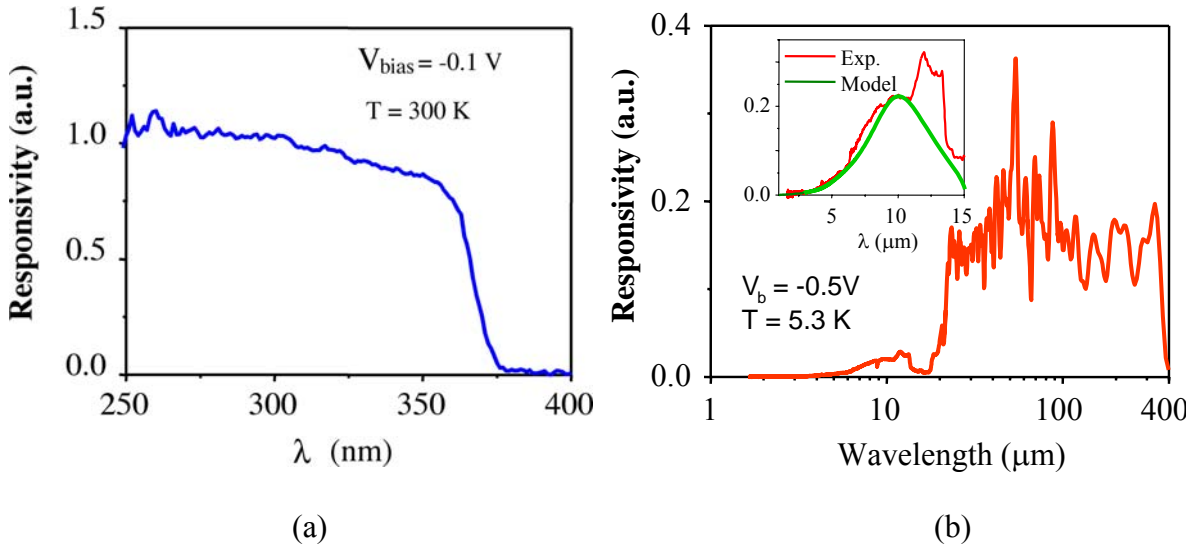


**Figure 4:** (a) UV/IR dual response of the detector, b) Calculated IR response of the detector, fitted with experimental results. The response at  $\sim 54 \mu\text{m}$  (5.5 THz) is due to the transition between  $1s$  and  $2p_{\pm}$  impurity levels of Si in GaN.

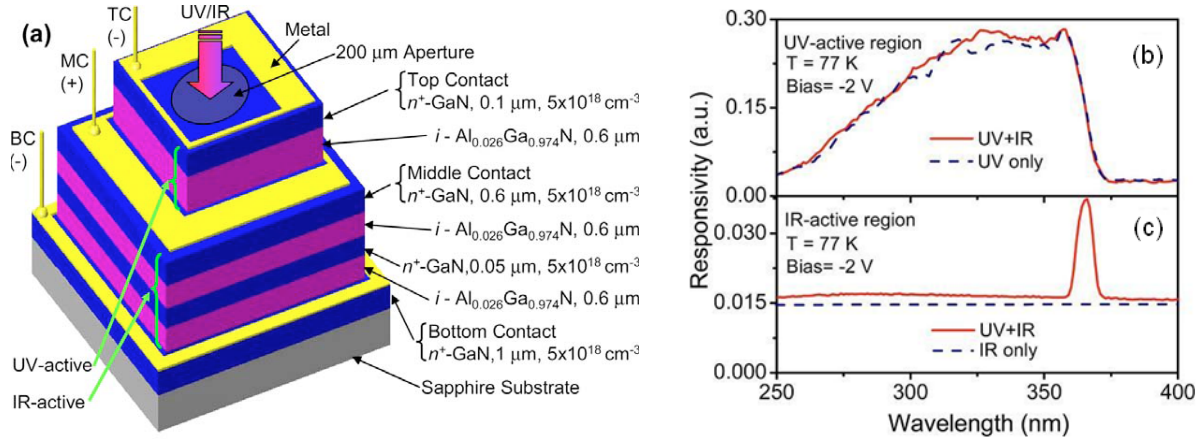


**Figure 5:** (a) Three contact structure for simultaneous dual-band response measurements showing separate active regions for UV and IR measurements, (b) simultaneously measured photocurrents (solid curves) from the UV-active region (TC-MC) and (c) the IR-active region (MC-BC) at 77 K when both UV and IR radiations were incident onto the detector.

In the spectral measurement setup, an optical chopper was used to modulate both the UV and IR radiations, providing the same modulation as in a typical application. A 200- $\mu\text{m}$ -diameter aperture was used to block the UV radiation leakage (i.e., entering the IR-active region without passing through the UV-active region) through the region around the MC. The responses from both active regions were obtained simultaneously at 77 K as shown in Figure 5(b, c). The solid curves show simultaneously measured photocurrents from the UV-active region [Fig. 5(b)] and

the IR-active region [Fig. 5(c)] at 77 K when both IR and UV radiations were incident onto the detector. The UV wavelength was varied between 250–400 nm, while IR radiation was fixed at 9.3  $\mu\text{m}$  (using the  $\text{CO}_2$  laser). The dashed curve in Fig. 5(b) represents the photocurrent from the UV active region when only the UV radiation was incident. Comparing the two curves, it is evident that there is no significant effect from IR radiation on the response, indicating a sole UV detection from the UV active region. The nearly constant response from the IR-active region, which is almost equal to the pure IR response [dashed line in Fig. 5(c)], is a good indication that the response is due to the fixed IR light and there is no effect from the UV radiation except for an exciton peak observed around 365 nm. The broad IR responses from both active regions obtained separately at 77 K show the free carrier response seen as a broad peak with a maximum near 11  $\mu\text{m}$ . The UV-active region did not show a measurable IR response under negative bias but did show a response under positive bias as expected. The detector can be further improved by the addition of more periods of GaN/GaN in the IR-active region and using interdigitated contacts in the UV active region.

### Published Papers and References:

1. G. Ariyawansa, M. B. M. Rinzan, M. Alevli, M. Strassburg, N. Dietz, and A. G. U. Perera, S. G. Matsik, A. Asghar and I. T. Ferguson, H. Luo, A. Bezinger, and H. C. Liu, “GaN/AlGaN ultraviolet/infrared dual-band detector”, *Appl. Phys. Lett.* 89, 091113 (2006).
2. A.G.U. Perera, G. Ariyawansa, M.B.M. Rinzan, M. Stevens, M. Alevli, N. Dietz, S.G. Matsik, A. Asghar, I.T. Ferguson, H. Luo, A. Bezinger, H.C. Liu, “Performance improvements of ultraviolet/infrared dual-band detectors”, *Infrared Physics & Technology* 50, 142(2007).
3. V. Bougrov, M. Levinshtein, S. Rumyantsev, and A. Zubrilov, in *Properties of Advanced Semiconductor Materials GaN, AlN, InN, BN, SiC, SiGe*, edited by M. E. Levinshtein, S. L. Rumyantsev, and M. S. Shur (Wiley, New York, 2001), p. 1.
4. M. Sumiya, K. Yoshimura, K. Ohtsuka, and S. Fuke, *Appl. Phys. Lett.* 76, 2098 (2000).
5. Ranga C. Jayasinghe, Gamini Ariyawansa, Nikolaus Dietz, A. G. Unil Perera, Steven G. Matsik, Hongbo B. Yu, Ian T. Ferguson, Andrew Bezinger, Sylvain R. Laframboise, Margaret Buchanan, and Hui Chun Liu, “Simultaneous detection of ultraviolet and infrared radiation in a single GaN/GaN heterojunction”, *OPTICS LETTERS*, Vol. 33, No. 21, 2422 (2008).